Improving purity of the radially polarized beam generated by a geometric phase retarder with spatially variable retardance

MAKSYM IVANOV[1], AIDAS MATIJOŠIUS[1], AND VIKTORIJA TAMULIENĖ[1]

[1] Laser Research Center, Vilnius University, 10 Sauletekio avenue, Vilnius, Lithuania, LT-10223
[*] Corresponding author: maks.ivannov@gmail.com

Compiled January 1, 2020

Geometric phase retarders—such as q-plates and S-waveplates—have found wide applications due to simplicity of operational principles and flexibility for the generation of azimuthally symmetric polarization states and optical vortices. Ellipticity of the polarization vector and phase of the generated beam strongly depend on the retardation of the plate. Real devices usually have retardation value slightly different than the nominated one. Previously unattended perturbation of the retardation leads to asymmetry in intensity distribution and variation of ellipticity of the local polarization vector of the generated beam. We elucidate that controlled and intentionally driven azimuthally variable, oscillating perturbation of the retardation reveals possibility to avoid distortions in the generated beam and leads to the recovery of the symmetrically distributed intensity and polarization (with zero ellipticity) of the beam. Described recovery of the desired polarization state could find application for generation of the high purity beam with azimuthally symmetric polarization, which local polarization ellipse has zero ellipticity.

http://dx.doi.org/10.1364/ao.XX.XXXXXX

1. INTRODUCTION

Increasing number of photonic applications employ vector beams with exotic polarization and phase distributions. For example, optical vortices are used in optical trapping [1, 2]. Radially/azimuthally polarized beams are used for electron bunch acceleration and compression [3–6], and laser material processing [7–10]. Among other methods these beams can be conveniently generated using a geometric phase retarder. The retarder is a quarter- and half-wave plate with variable orientation of the fast axis. It can be manufactured by gluing together pieces of waveplates – axially-symmetric plates [11, 12], using liquid crystals – q-plates [13, 14], and by writing nano-grating inside a glass plate – S-waveplate [15, 16].

Radially (azimuhally) polarized beam can be considered as a superposition of two vortex beams of opposite directions of vorticity and circulations of the polarization vector [17–21]. Since the beam generated on the retarder is a superposition of two vortex beams, then it is very sensitive to the small perturbations of (i) retardance and of (ii) orientation of variable optical axis of the plate. (i) $\lambda/2$ retardation value ensures (a) equal intensities of right- (left-)hand circularly polarized (R and L, respectively) vortex components of the beam, and (b) coincidence/match of locations of vortices within these components; (a) and (b) ensures "linear" (meaning zero ellipticity of the local polarization vector) polarization of the converted beam. (ii) Gradual change of the orientation of the optical axis of a geometric phase retarder ensures (c) constant advance of the vortex phase in the L and R components of the beam, and (d) constant rotation of orientation of the local polarization vector of the generated beam, hence its alignment in radial (azimuthal) pattern. It is technically challenging to create a geometric-phase retarder plate with exactly half waveplate (π) retardation at every point on the plate (i.e. spatially homogeneous retardation). Majority of techniques especially at their early production years, have been producing plates with retardation which differs from π by up to 10% at different places on the plate (i.e. spatially inhomogeneous retardation). Previously, effect of retardation perturbation on the generated beam was studied only partially. D'Errico et al. [22] considered features of a vector beam generated by a geometric phase retarder with retardation perturbed homogeneously only, which usually is not the case in the experiment. Moreover, methods for recovery of the desired polarization distribution generated with the perturbed retarder were not suggested.

The effect of (ii) perturbation of orientation of the optical axis of the retarder will be studied elsewhere. In this article, we investigate the effect of (i) perturbation of retardation of the geometric phase retarder, considering both homogeneous and inhomogeneous perturbation, on the polarization, phase, and intensity structure of the generated beam. Our theory suggests, and experiment confirms, that perturbation of retardation leads to the off-axis shift of vortices in the L and R components. This in turn results in break in the symmetry of intensity, ellipticity of local polarization vector, and phase distribution of the converted beam. However, it appears that inhomogeneous perturbation of retardation in the form of azimuthally asymmetric oscillations around half-wave plate value might lead to recovery of

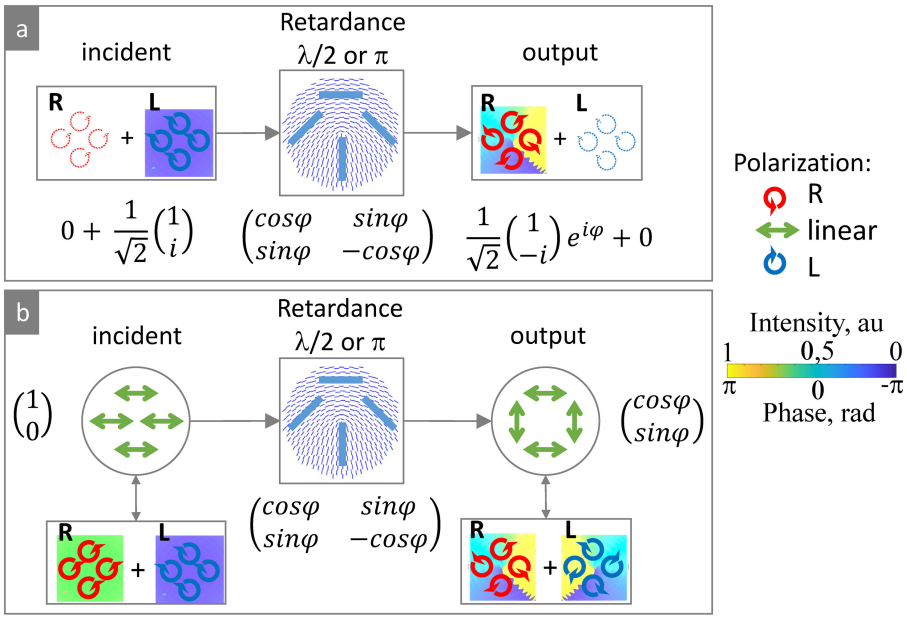

Fig. 1. Schematic of polarization, phase, and angular momenta conversion for incident (a) circularly polarized and (b) linearly polarized beams. Arrows and the Jones matrices at the bottom of the arrows show polarization state; phase is shown at the background. Right hand circular polarization state is shown by red color, linear - by green, left hand circular - by blue color. Components shown by dotted lines have zero intensity. Retardance of the S-waveplate and orientation of its optical axis are shown in the middle together with its Jones matrix.

the symmetrically distributed intensity, phase, and desired zero ellipticity of the local polarization vector of the beam upon its free space propagation. These results are of importance for understanding the reasons of differences between expected and obtained quality of the generated beams. They can be used as alternative approach for the generation of high purity radially (azimuthally) polarized beams, and are of importance for high precision experiments, such as electron bunch compression using radially polarized beams.

2. POLARIZATION-PHASE CONVERSION OF THE BEAM ON A GEOMETRIC PHASE RETARDER

Fig. 1 schematically shows the process of conversion of the beam on the geometric phase retarder. We consider the retarder which induces half-wave retardance and which optical axis rotates 180 degrees over full azimuthal angle, i.e. topological charge of the retarder is $q = 1/2$ [13]. The Jones matrix of the unperturbed retarder with π retardation is given by:

$$M_q = \begin{bmatrix} \cos(\varphi) & \sin(\varphi) \\ \sin(\varphi) & -\cos(\varphi) \end{bmatrix}, \quad \textbf{(1)}$$

where φ is the azimuthal angle of a polar coordinate system. The middle part of Figure 1 schematically demonstrates orientation of the optical axis of the retarder, its retardation (exactly $\lambda/2$ or π), and the Jones matrix M_q. We discuss the action of the retarder on different input polarization states. The Jones vectors of horizontally (X), vertically (Y) linearly, and left-handed (L) and right-handed (R) circularly polarized states are given by:

$$E_X = \frac{1}{\sqrt{2}}\begin{bmatrix}1\\0\end{bmatrix}; E_Y = \frac{1}{\sqrt{2}}\begin{bmatrix}0\\1\end{bmatrix}; \quad E_L = \frac{1}{\sqrt{2}}\begin{bmatrix}1\\i\end{bmatrix}; E_R = \frac{1}{\sqrt{2}}\begin{bmatrix}1\\-i\end{bmatrix}, \quad \textbf{(2)}$$

respectively.

Left part of Fig. 1 labelled 'incident' shows incident polarization state and corresponding Jones vector. A Gaussian beam converted by such a retarder transforms to a doughnut shaped beam. Right part of Fig. 1 labelled 'output' shows polarization state of the converted beam. Orientation of arrows shows phase of the beam, with the phase map at the background. The conversion is accompanied by the following transformation of polarization and phase of the beam: Fig. 1a the initial left (right) circular polarization (with $|l| = 0$) transforms to right (left) circular polarization, the beam acquires vortex phase with topological charge $|l| = 1$, as evident from the $e^{i\varphi}$ component in the Jones matrix and by phase distribution in the corresponding subimage. With the notations of Eqs. (1), (2) we can write:

$$M_q E_L = E_R \exp(i\varphi);\ M_q E_R = E_L \exp(-i\varphi). \quad \textbf{(3)}$$

Fig. 1b shows that the initial linear polarization becomes azimuthal if the retarder is oriented perpendicularly to the orientation of the incident linear polarization, and radial if this orientation is parallel (not shown). The output beam is a superposition of two vortices with opposite phases, so the total phase of the beam remains vortex-free, e.g. the amplitude functions

$$M_q E_X = E_{RP};\ M_q E_Y = E_{AP}, \quad \textbf{(4)}$$

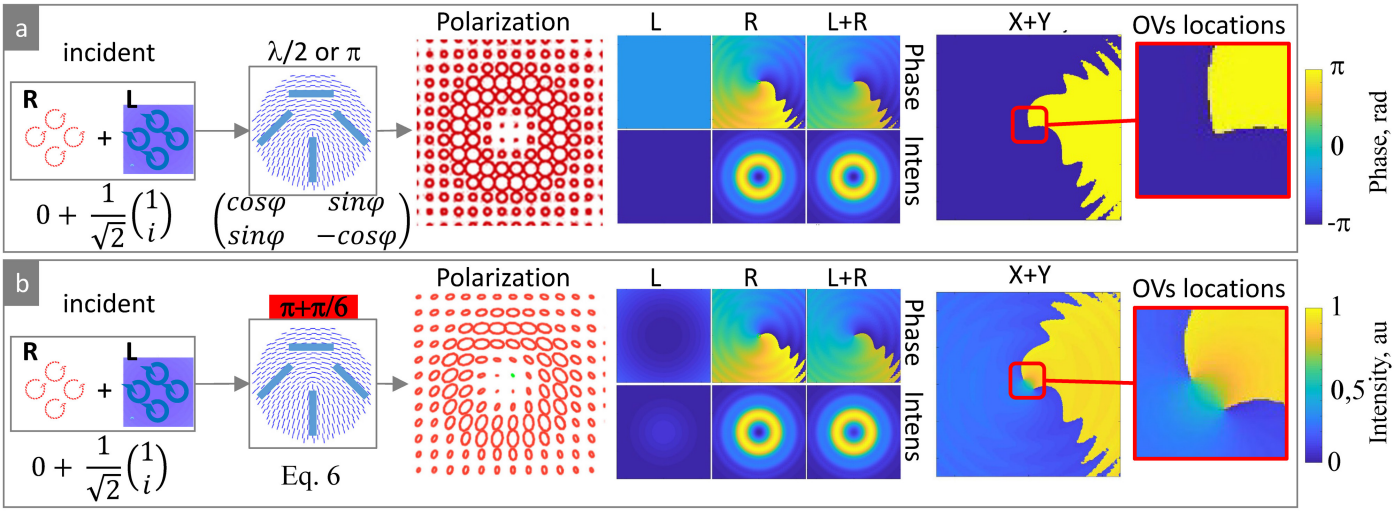

Fig. 2. Modelling results of polarization, phase, and intensity distribution of the beam converted by the geometric phase retarder with (a) ideal π retardation and (b) perturbed retardation $\pi + \pi/6$. Circularly polarized Gaussian beam is incident. Arrows and the Jones matrices at the bottom of the arrows show polarization state; phase is shown at the background. Components shown by dotted lines have zero intensity. Retardance of the S-waveplate, orientation of its optical axis, and its Jones matrix are also shown. Polarization of the converted beam is shown in the column "Polarization". It is color coded as in Fig. 1. Columns labelled by L, R, $L+R$, and $X+Y$ show intensity and phase of left-hand, right-hand, combined left- and right-hand circularly polarized components, and of combined horizontally and vertically polarized components of the beam, respectively. Locations of optical vortices in the combined beam are shown in the rightmost column.

where

$$E_{RP} = \frac{1}{\sqrt{2}}\begin{bmatrix}\cos(\varphi)\\ \sin(\varphi)\end{bmatrix};\ E_{AP} = \frac{1}{\sqrt{2}}\begin{bmatrix}\sin(\varphi)\\ -\cos(\varphi)\end{bmatrix} \tag{5}$$

describe the radial and azimuthal polarizations, respectively.

3. HOMOGENEOUS RETARDATION

A. Circularly polarized input beam for optical vortex generation

A.1. Unperturbed case

In this case, retardance of the plate is homogeneous and has π value.

Phase and Intensity. Fig. 2a in columns with corresponding labels shows phase and intensity distribution in the L and R polarized components of the converted beam. Initially incident L component after conversion has zero intensity. All the intensity is in the R component which has a vortex phase. Intensity distribution is symmetric.

Polarization. Upon conversion polarization vector preserves initial value of ellipticity but changes its sign. Incident L polarization becomes R with homogeneously distributed ellipticity and orientation of polarization ellipses as shown in column 'Polarization' in Fig. 2a.

Location of vortices. Output beam was decomposed to X- and Y-polarized components, which phase is shown in the column 'X+Y' in Fig. 2a. Vortices from orthogonally polarized components have the same locations within the beam, as seen in the rightmost 'OVs locations' column in Fig. 2a.

A.2. Perturbed case

Retardation of the geometric phase retarder can vary from π value due to manufacturing errors, or if the incident wavelenght is different than the nominated one. The converter with the perturbed retardation is represented by the Jones matrix M_u:

$$M_u = \begin{bmatrix}\cos(q\varphi) & -\sin(q\varphi)\\ \sin(q\varphi) & \cos(q\varphi)\end{bmatrix} \times \begin{bmatrix}1 & 0\\ 0 & \exp(i\Delta)\exp(iu)\end{bmatrix}\begin{bmatrix}\cos(q\varphi) & \sin(q\varphi)\\ -\sin(q\varphi) & \cos(q\varphi)\end{bmatrix}. \tag{6}$$

From Eq. (6) we obtain:

$$M_u = \frac{a}{2}M_q + \frac{b}{2}M_I, \tag{7}$$

where

$$a = [1+\exp(iu)],\ b = [1-\exp(iu)] \tag{8}$$

and $M_I = \begin{bmatrix}1 & 0\\ 0 & 1\end{bmatrix}$ is a unity matrix, M_q is the matrix of the unperturbed retarder (Eq. (1)). q describes rotation of optical axis of the plate (we consider $q = 1/2$), Δ is the retardation of the plate (we consider that $\Delta = \pi$) and u describes perturbation of the retardation. When $u = 0$, $b = 0$ and $M_u = M_q$. When $u \neq 0$, the effect of the plate on X, Y, L, R, and elliptic polarizations can be described by amplitude functions:

$$M_u E_X = \frac{a}{2}E_{RP} + \frac{b}{2}E_X,\ M_u E_Y = \frac{a}{2}E_{AP} + \frac{b}{2}E_Y, \tag{9}$$

$$M_u E_L = \frac{a}{2}E_R\exp(i\varphi) + \frac{b}{2}E_L,$$
$$M_u E_R = \frac{a}{2}E_L\exp(-i\varphi) + \frac{b}{2}E_R, \tag{10}$$

and

$$M_u E_e = \frac{1}{2}\left(\ acE_R\exp(i\varphi) + adE_L\exp(-i\varphi) + bcE_L + bdE_R\right), \tag{11}$$

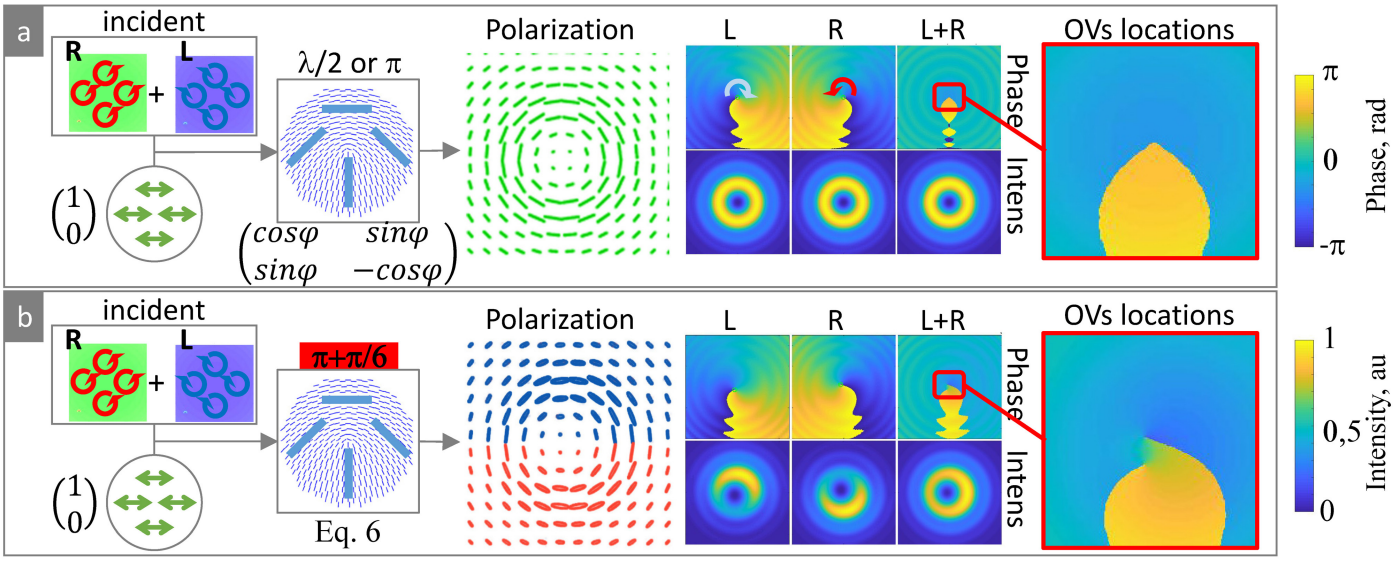

Fig. 3. Modelling results of polarization, phase, and intensity distribution of the beam converted by the geometric retarder with (a) ideal π retardation and (b) perturbed retardation $\pi + \pi/6$. Linearly polarized Gaussian beam is incident (which is decomposed to L and R polarized components). Arrows and the Jones matrices at the bottom of the arrows show polarization state; phase is shown at the background. Components shown by dotted lines have zero intensity. Retardance of the S-waveplate, orientation of its optical axis, and its Jones matrix are also shown. Polarization of the converted beam is shown in the column "Polarization". It is color coded as in Fig. 1. Columns labelled by L, R, $L+R$, and $X+Y$ show intensity and phase of left-hand, right-hand, combined left- and right-hand circularly polarized components, and of combined horizontally and vertically polarized components of the beam, respectively. Locations of optical vortices in the combined beam are shown in the rightmost column.

respectively. Where c and d are weights of L and R polarized components, respectively. As seen from Eqs. (9) and (10) the output beam is a superposition of the desired polarization state (as from the unperturbed case) and some coherent background polarized as the incident beam. Fig. 2b shows the results of modelling to demonstrate this as described below. Here we consider homogeneous retardation of the retarder, which differs from π by extra $\pi/6$, i.e. $u = \pi/6$, see Eqs.(7) and (8).

Phase and Intensity. In contrary to the unperturbed case, when retardation of the plate differs from π, both L and R components of the resulting beam are nonzero, as shown in the Fig. 2b in the columns with corresponding labels. But only component with polarization state orthogonal to that of the incident, which in our case is R, acquires vortex phase, while L component is a vortex-free background. Therefore, the beam with vortex phase and doughnut intensity can be spatially separated from the resultant superposition by a polarizer. Intensity of the converted beam remains symmetric.

Polarization. Column 'Polarization' in Fig. 2b shows that even though ellipticity of the incident polarization was homogeneous, ellipticity and orientation of the polarization ellipses of the converted beam become inhomogeneous, i.e. spatially variable. Nonetheless, this elliptical polarization can be decomposed to L and R components to separate the homogeneously polarized vortex beam, as mentioned previously.

Location of vortices. Coherent background in the generated superposition of vortex beam and non-vortex background shifts vortex from the center of the beam [23]. This is explicitly shown by the decomposing the resulting beam into the X- and Y-polarized components (Fig. 2b columns 'X+Y' and 'OVs locations').

Generation of optical vortex beam using spatial separation by polarization was recently demonstrated in an octave spanning range [16].

B. Linearly polarized input beam for generation of radial/azimuthal polarization

B.1. Unperturbed case

In this case, retardance of the plate is homogeneous and has π value.

Phase and Intensity. Incident linear polarization is considered as superposition of L and R components, as it is schematically shown in the 'incident' column of Fig. 3a. Upon conversion both incident, L and R, components flip handedness and acquire vortex phase as shown in the columns 'L' and 'R'. Vortices in these components have orthogonal direction of vorticity. L and R components have equal amplitudes and symmetric intensity distributions. The generated azimuthally polarized beam is vortex-free, it has plane phase (Fig. 3a column 'L+R').

Polarization. Polarization vector is oriented azimuthally, as shown in the column 'Polarization' in Fig. 3a. Ellipticity of the polarization vector of the resultant beam is zero (i.e. polarization is linear at every point).

Location of vortices. The rightmost 'OVs locations' column in Fig. 3a shows that the vortices from orthogonally polarized L and R components have the same locations within the beam. Then vortex phase is cancelled such that the resultant phase of the azimuthally polarized beam is vortex free.

B.2. Perturbed case

Here we consider homogeneous retardation of the retarder, which differs from π by extra $\pi/6$, i.e. $u = \pi/6$, see Eqs. (7) and (8). Fig. 3b demonstrates the effect of such perturbation on the generation of radially/azimuthally polarized beam.

Phase and Intensity. Upon conversion both incident, L and R, components flip handedness of polarization and acquire vor-

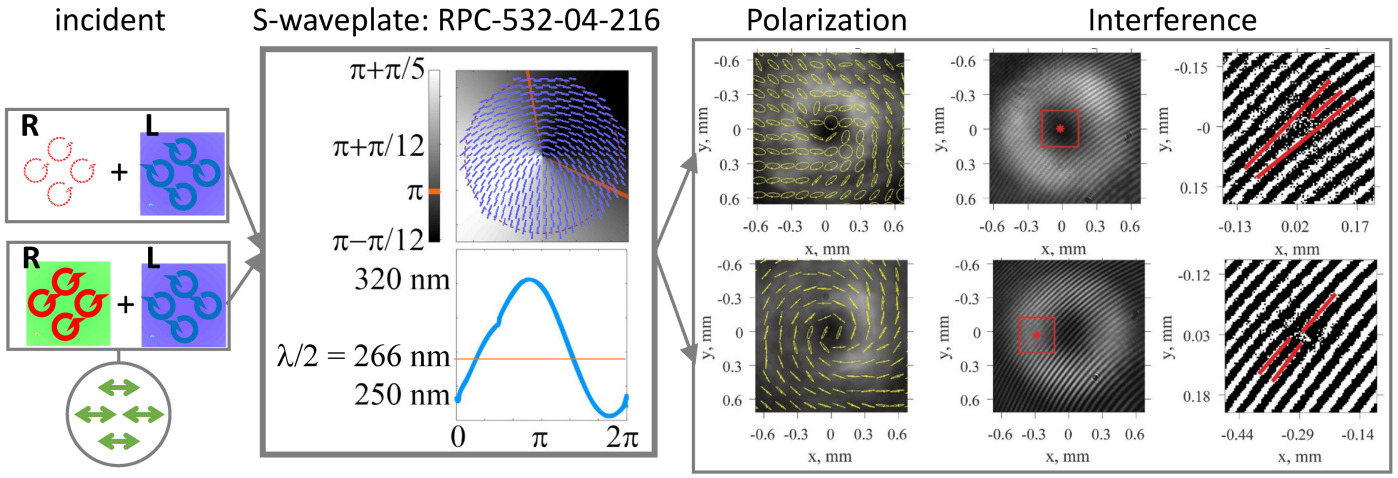

Fig. 4. Experimentally retrieved polarization (using Stokes parameters [24–26]) and locations of vortices in the beam converted on the S-waveplate (RPC-532-04-216) in the case of circularly (upper part) and linearly (lower part of the figure) polarized incident Gaussian beam. Vortex location is marked by red star. Rightmost column shows magnified area shown by the red square in the subimages with interference. Polarization of the reference beam for interference is vertical, Y.

tex phase as shown in the columns 'L' and 'R' of Fig. 3b. In contrary to the unperturbed case, the L and R components, and combined resultant beam have asymmetric intensity distributions (Fig. 3b columns 'L', 'R', and 'L+R', respectively). Total phase of the generated azimuthally polarized beam is *not* vortex-free in this case.

Polarization. Column 'Polarization' in Fig. 3b shows that even though the polarization of the incident beam was homogeneous, the converted beam becomes inhomogeneously polarized, i.e. ellipticity of the local polarization ellipse spatially varies. It changes from the left-hand at the upper part of the beam to the right-hand elliptically polarized at the lower part. Polarization ellipses remain orientated azimuthally because its orientation depends on the orientation of the optical axis of the geometric phase retarder only.

Location of vortices. Each of the L and R components is superposition of vortex beam and vortex-free background (as explained in the section A). This leads to the shift of the vortices in these component from the center of a beam [23], as explicitly shown in the rightmost 'OVs locations' column in Fig. 3b. This difference of locations of vortices does not allow for full cancellation of the vortex phase in the resultant beam and causes above mentioned spatially variable ellipticity of the local polarization vector.

4. INHOMOGENEOUS RETARDATION

A. Experimental observations

In practice, it is hard to manufacture an element with spatially homogeneous retardation. For example, experimentally measured retardation of the nano-structured geometric phase retarder (S-waveplate "RPC-532-04-216") manufactured for the central wavelength $\lambda = 532$ nm is shown in Fig. 4 in the column with corresponding label. Its retardation oscillates around π value from $\pi - \pi/12$ to $\pi + \pi/5$ and has a variable profile. As a result, beam acquires spatially variable ellipticity (Fig. 4 column 'Polarization'). This results in appearance of vortex phase in the beam, as seen from the interference pattern shown the corresponding column in Fig. 4. Interference patterns demonstrate appearance of the vortex phase in the Y polarized component of the beam, which would be vortex free if the retardation was π. Position of the vortex is shifted further from the center of the beam than expected from the previous sections. Therefore, the following question we aim to answer is: What effect the inhomogeneous retardation which oscillates around π value has on the beam conversion?

B. Oscillating (sinusoidal) retardation

Experimentally retrieved oscillating profile of retardation of the S-waveplate has led to consideration of sinusoidal profiles of retardation of the geometric phase retarder. Therefore, the following retardation profile of the plate is considered: $u = \alpha \sin(j\varphi)$ (to be used in Eq. (8)) as shown in the 'Retardation' columns in Fig. 6 and 8, where j is the period of oscillation, φ is the azimuthal angle changing from 0 to 2π, and α is the depth of perturbation of retardation. $\alpha = \pi/6$ was chosen to be similar to the experimentally retrieved value from the previous subsection.

In this case, we make use of Jacobi-Anger expansion: $\exp(iu) = \exp(i\alpha \sin(j\varphi)) = \sum_{n=-\infty}^{\infty} J_n(\alpha) \exp(inj\varphi)$, where J_n is the Bessel function. Moreover, $J_{-n}(\alpha) = (-1)^n J_n(\alpha)$. We insert the expansion into coefficients a and b of Eqs. (7) and (8):

$$a = 1 + \exp(iu) = 1 + J_0(\alpha) + J_1(\alpha) 2i \sin(j\varphi) + J_2(\alpha) 2\cos(2j\varphi) + \dots \quad (12)$$

and

$$b = 1 - \exp(iu) = 1 - J_0(\alpha) - J_1(\alpha) 2i \sin(j\varphi) - J_2(\alpha) 2\cos(2j\varphi) + \dots \quad (13)$$

When $\alpha < 1$, $J_0(\alpha) \approx 1$ and we note the difference in Eqs. (12) and (13): in Eq. (12) the main contribution is made of $(1 + J_0(\alpha))$ and the field is modulated by the following $\sin(j\varphi)$ and higher terms. In Eq. (13), the term $(1 - J_0(\alpha))$ vanishes, and the modulations are more prominent. Another important aspect is that during the free-space propagation the higher order oscillations diffract out faster than lower order oscillations (Fig. 5). This allows us to leave only J_0 and J_1 terms in expansions Eqs. (12) and (13) and neglect oscillations of the higher order. Modelling was

performed both using the approximation and without it showing no significant difference. Fig. 5 demonstrates normalized intensity of the vortex, R, and background components, L, (the latter are labelled by the corresponding j number). Size of the vortex component is 100 μm, size of the background component is 2.5 times bigger for $j = 8$. Therefore, upon beam propagation high-order component diffracts faster and leaves the central part of the beam. This has important consequence for the generation of the beam with azimuthal/radial polarization, as discussed below.

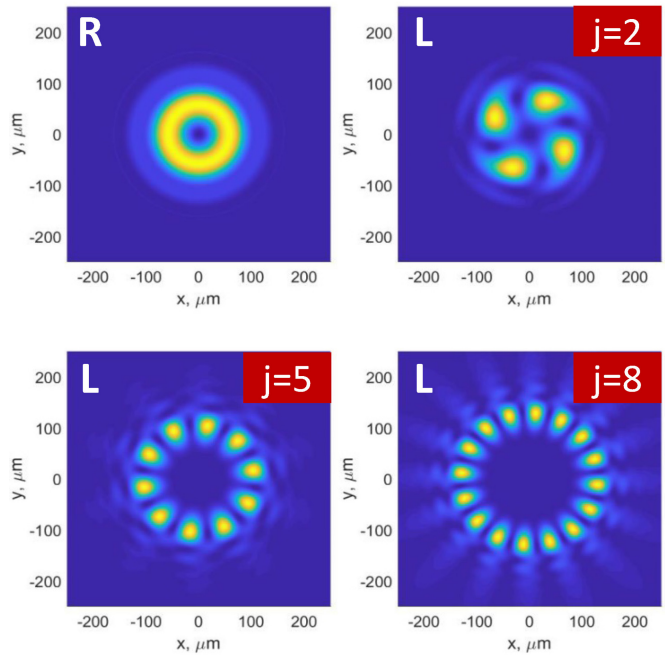

Fig. 5. Size of the vortex, R, component is 100 μm. Sizes of the background, L, components for $j = 2, 5, 8$ (as specified in the labels) are 150, 200, 250 μm, respectively. Propagation distance $z = 1$ cm, size of the initial Gaussian beam is 100 μm, $\lambda = 532$ nm.

B.1. Retardance oscillating as $u = \alpha \sin(j\varphi)$*, where* $j = 1$

Figure 6 demonstrates the polarization, phase, and intensity of the beam generated by the geometric phase retarder with sinusoidally variable profile of retardation with amplitude $\alpha = \pi/6$ and period $j = 1$. Figure 7 demonstrates evolution of the generated beam upon its free space propagation.

Circularly polarized *(L) incident beam:*

Phase and intensity. Similarly to the case of homogeneously perturbed retarder, the resulting beam is a superposition of L and R components. However, in the case of inhomogeneous retardation, both L and R components of the resulting beam carry optical vortices (upper part of Fig. 6). For $j = 1$, size of both, L and R, polarized components and their divergence are similar, as explicitly shown in the upper part of Fig. 7. The coherent background affects the total intensity distribution making it asymmetric.

Polarization. The generated beam has spatially variable ellipticity and orientation of polarization ellipses (upper part of Fig. 6 'Polarization').

Linearly polarized *(R+L) incident beam:*

Phase and intensity. As previously, linearly polarized incident beam is considered as a superposition of L and R polarized components. Each of these components, after conversion on the retarder, is a superposition of vortex and background components, both of which carry optical vortices as demonstrated above. Therefore, intensity distribution of the L and R components is strongly asymmetric (lower part of Fig. 6).

Polarization. Polarization ellipses of the generated beam have spatially variable ellipticity (lower part of Fig. 6 'Polarization'). Polarization is right-hand elliptical (shown by blue color) at the upper and lower parts of the beam where the deviations of the retardation from π is maximal and it is linear (shown by green color) at places where the plate has π retardation. Lower part of Fig. 7 demonstrates evolution of the polarization distribution upon beam propagation. Polarization remains elliptical with variable ellipticity of the local polarization vector.

Location of vortices. Vortices from the orthogonally polarized components have different locations within the beam, as explicitly shown in the rightmost 'OVs locations' column in Fig. 6. This difference of locations of vortices does not allow for full cancellation of the vortex phase in the resultant beam.

B.2. Retardance oscillating as $u = \alpha \sin(j\varphi)$*, where* $j = 8$

Figure 8 demonstrates the polarization, phase, and intensity of the beam generated by the geometric phase retarder with sinusoidally variable profile of retardation with amplitude $\alpha = pi/6$ and period $j = 8$. Figure 9 demonstrates evolution of the generated beam upon its free space propagation.

Circularly polarized *(L) incident beam:*

Phase and intensity. Upper part of Fig. 8 shows intensity and phase of the L and R components of the beam after conversion on the retarder. Background component, L, carry a number of optical vortices and resembles a 16 petal structure. This is because retardation profile of the geometric phase retarder 16 times crosses π value along the full azimuthal angle. Contrary to the previously described case ($j = 1$), in the case of $j = 8$ the multi-vortex background component, L, diffracts faster than the vortex component, R, upon propagation. This is explicitly shown in the upper part of Fig. 9 (and in Fig. 5). Therefore, only periphery of the generated beam is affected, while the main (brightest) ring of the light remains intact (upper part of Fig. 8).

Polarization. Since only periphery of the beam is affected, the polarization of the generated beam remains homogeneous, circularly polarized, on the brightest ring of light (upper part of Fig. 8 column 'Polarization').

Linearly polarized *(R+L) incident beam:*

Phase and intensity. As demonstrated above in the case of circularly polarized incident beam, after conversion on the plate with retardation oscillating $j = 8$ times around π value, the size and divergence of the vortex and background components are different. Thereby additional vortices appearing in the beam affect mostly periphery of the generated beam. Therefore, the brightest ring of light remains almost intact. Lower part of Fig. 9 explicitly demonstrates recovery of symmetry of intensity distribution upon beam propagation due to different divergences of vortex and multi-vortex background components of the beam.

Polarization. Since only periphery of the beam is affected, the polarization of the generated beam remains homogeneous, linearly polarized, on the brightest ring of light (lower part of Fig. 8 column 'Polarization'). Lower part of Fig. 9 demonstrates evolution of the polarization distribution upon beam propagation. As the multi-vortex background component diffracts faster

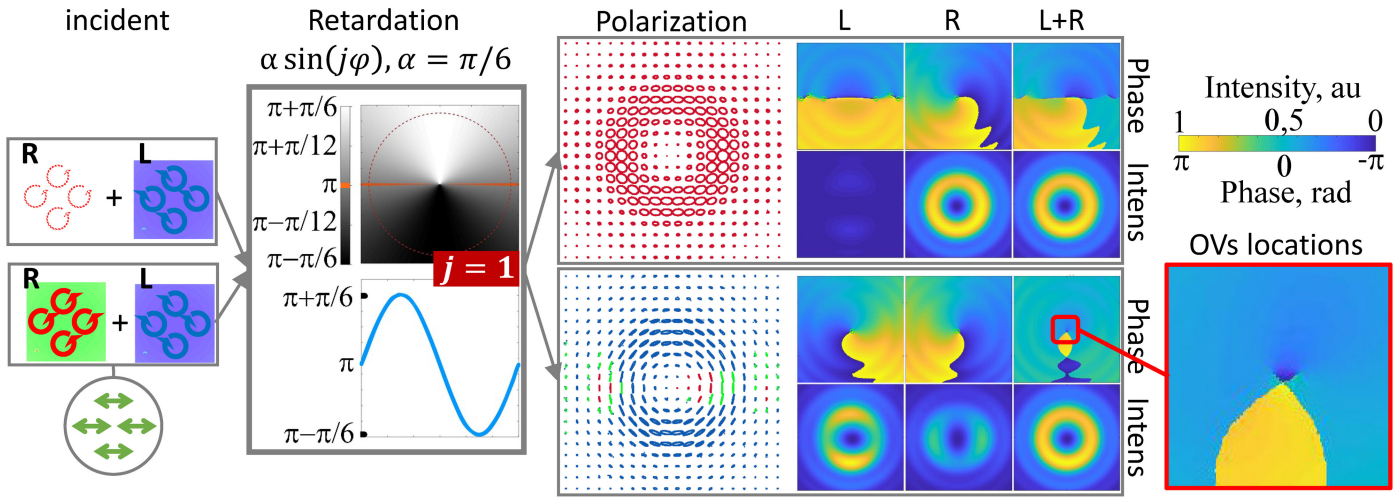

Fig. 6. Modelling results of polarization, phase, and intensity distribution of the beam converted by the geometric phase retarder with sinusoidal profile of retardation, $u = \alpha \sin(1\varphi)$. Conversion of circularly polarized incident Gaussian beam is shown in the upper part, of linearly polarized - in the lower part. Retardance distribution and its profile along full azimuthal angle (blue curve) are also shown. Polarization of the converted beam is shown in the column "Polarization". It is color coded as in Fig. 1. Columns labelled by L, R, and $L + R$ show intensity and phase of left-hand, right-hand, combined left- and right-hand circularly polarized components, respectively. Locations of optical vortices in the combined beam are shown in the 'OVs locations' column.

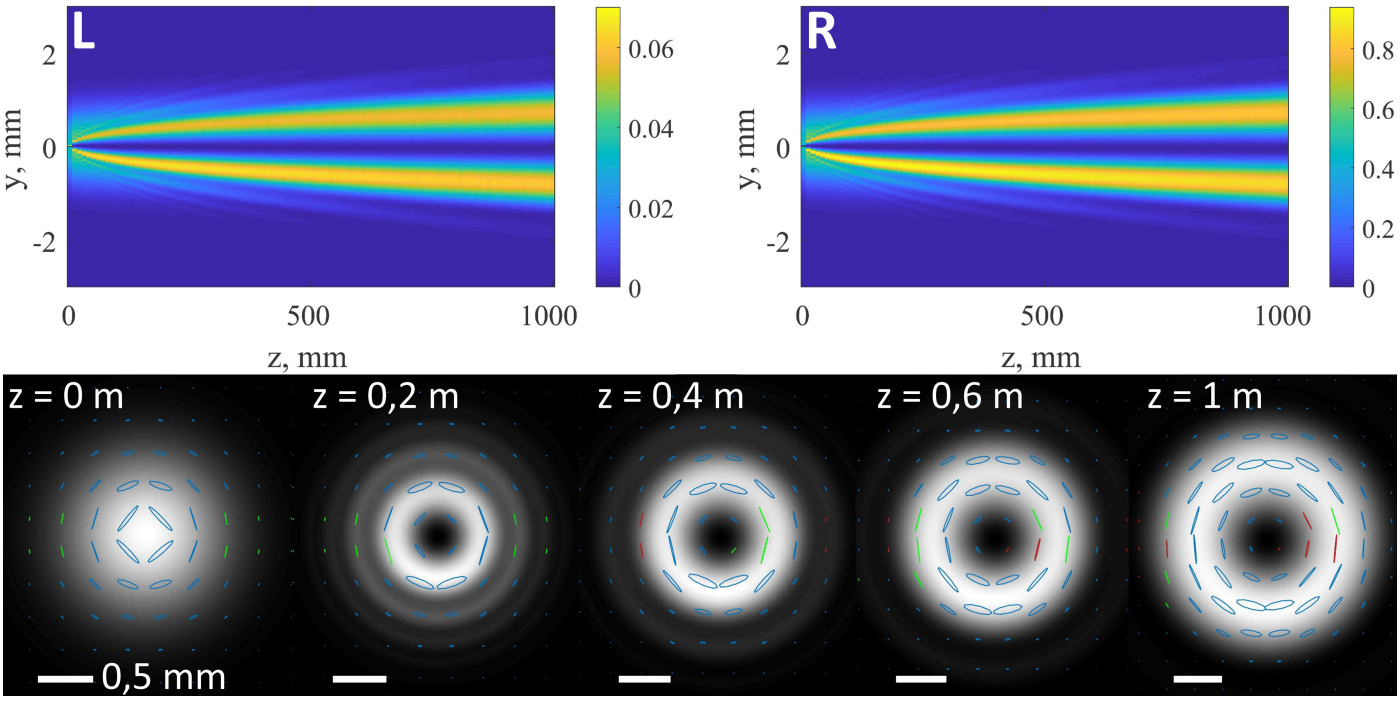

Fig. 7. Upper part: Normalized intensity distributions in L and R components of the beam versus propagation distance, z, is shown. x coordinate is taken at 0 mm. Circularly polarized beam was incident on the plate with $u = \alpha \sin(1\varphi)$ profile of retardation. Note similar divergence of two components.
Lower part: Snapshots of intensity and polarization of the beam at specified propagation distances, z, are shown. Right (left) hand circular polarization is shown by red (blue) color, linear - by green. Linearly polarized beam was incident on the plate with $u = \alpha \sin(1\varphi)$ profile of retardation.

and leaves the beam, the local polarization vector becomes linear, with zero ellipticity (shown by green color). The desired, in this case azimuthal polarization, is recovered.

Location of vortices. Since only periphery of the beam is affected, vortices of L and R components are located much closer to each other (Fig. 8 'OVs locations'). This leads to almost full cancellation of the vortex phase in the resultant beam (Fig. 8 column 'L+R'), to recovery of symmetric ring of light (Fig. 9 '$z = 1$ m'), and to recovery of the desired polarization state with zero ellipticity of the local polarization vector on the ring of light

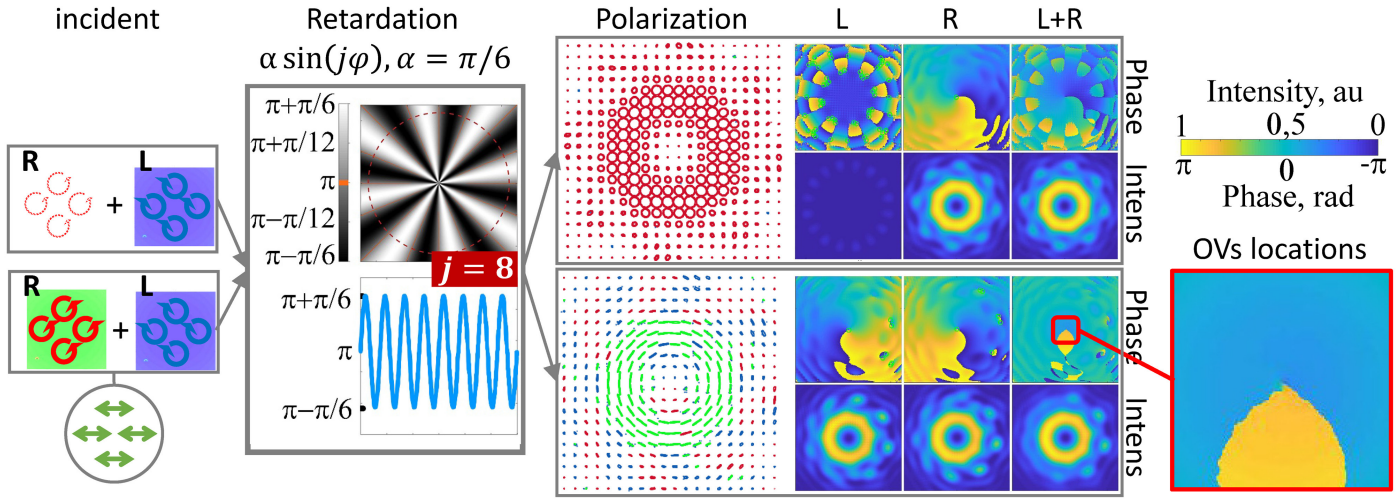

Fig. 8. Modelling results of polarization, phase, and intensity distribution of the beam converted by the geometric phase retarder with sinusoidal profile of retardation, $u = \alpha \sin(8\varphi)$. Conversion of circularly polarized incident Gaussian beam is shown in the upper part, of linearly polarized - in the lower part. Retardance distribution and its profile along full azimuthal angle (blue curve) are also shown. Polarization of the converted beam is shown in the column "Polarization". It is color coded as in Fig. 1. Columns labelled by L, R, and $L + R$ show intensity and phase of left-hand, right-hand, combined left- and right-hand circularly polarized components, respectively. Locations of optical vortices in the combined beam are shown in the 'OVs locations' column.

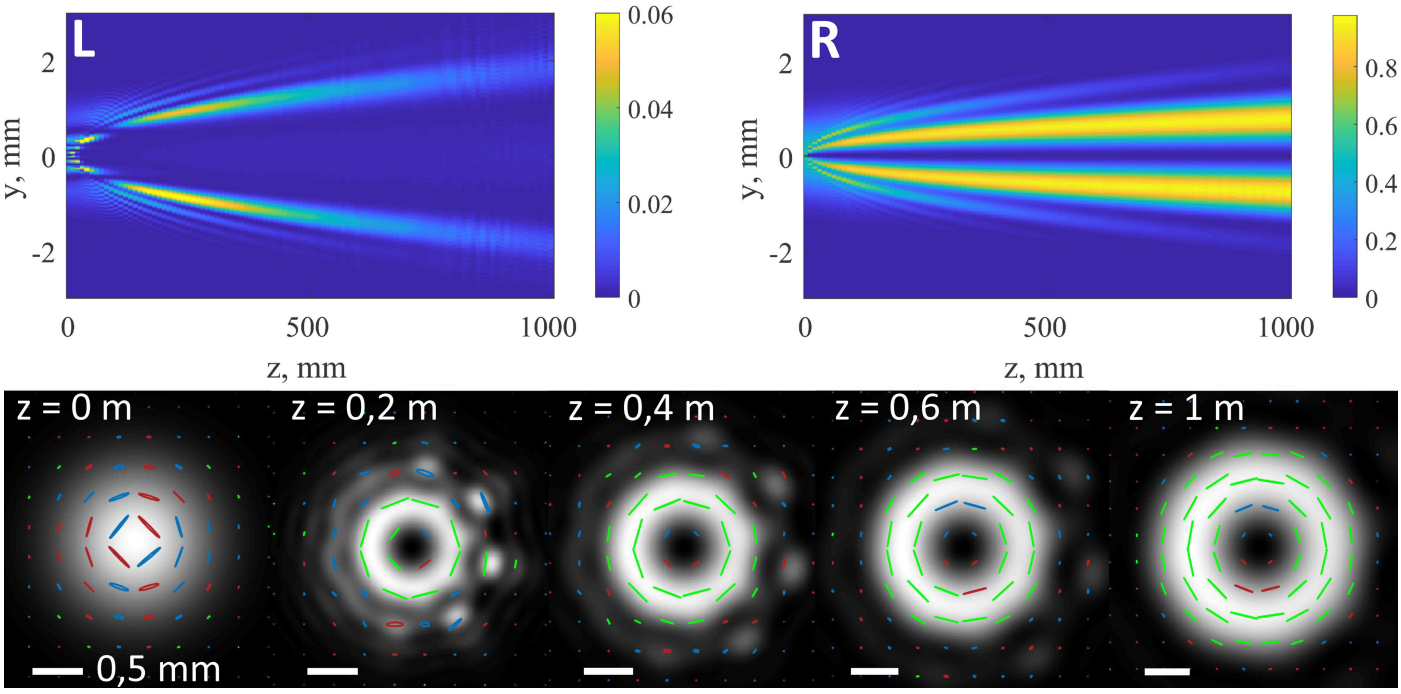

Fig. 9. Upper part: Normalized intensity distributions in L and R components of the beam versus propagation distance, z, is shown. x coordinate is taken at 0 mm. Circularly polarized beam was incident on the plate with $u = \alpha \sin(8\varphi)$ profile of retardation. Note different divergence of two components.
Lower part: Snapshots of intensity and polarization of the beam at specified propagation distances, z, are shown. Right (left) hand circular polarization is shown by red (blue) color, linear - by green. Linearly polarized beam was incident on the plate with $u = \alpha \sin(8\varphi)$ profile of retardation.

(Fig. 9 'z = 1 m').

Therefore, even though the geometric phase retarder has strongly perturbed retardation, for $j > 5$, locations of vortices in the L and R components almost coincide, then the local polarization vector of the generated beam acquires homogeneous (zero) ellipticity, close to that in the case of ideal homogeneous retardation with π value.

5. CONCLUSION

Conversion of the beam consisting of superposition of two orthogonal circularly polarized components on the geometric

phase retarder was considered. (1) When the retarder induces spatially *homogeneous half-wave retardation* each of the circularly polarized components acquire vortex phase. In the case of linearaly polarized beam incident on the retarder the resulting beam is vortex free, azimuthally/radially polarized with symmetric intensity distribution. (2) When the retarder induces spatially *homogeneous retardation which differs from half-wave retardation* then each of the circularly polarized components are superposition of vortex and background components. Interplay between these components results in the shift of position of vortices from the center of the beam (mismatch in their locations). This leads to azimuthally/radially aligned polarization with variable ellipticity of the local polarization ellipse, asymmetric intensity and phase distribution. (3) When the retarder induces spatially *inhomogeneous retardation* which *oscillates* around half-wave retardation then each of the circularly polarized components are superposition of two vortex components. (3a) When this oscillation is "slow" (<2 times around π value), then the divergence of two vortex components is similar. Interplay between these components results in, shift of vortices within orthogonal circularly polarized components, thus asymmetric beam with variable ellipticity of local polarization vector, similarly to the above described (2) case. (3b) When oscillation of retardation profile around π value is fast (>5 times), then the divergence of two vortex components of each orthogonal circularly polarized components of the beam are different. Upon propagation low intensity multi-vortex component diverges faster (then the single vortex component) and converges to the periphery of the beam. Therefore, vortices within orthogonal circularly polarized components remains to be located in the center of the beam. Thus resulting beam acquires symmetric intensity distribution and radial/azimuthal polarization with zero ellipticity of the local polarization ellipse, similarly to the (1) case of geometric phase retarder with homogeneous half-wave retardation.

Therefore, intentional spatial variation of the retardation of the geometric phase retarder in the $\alpha \sin(j\varphi)$ form might be an alternative technology for the generation of beams with radial/azimuthal polarization when homogeneous retardation is not achievable on practice.

6. DISCLOSURES

The authors declare no conflicts of interest.

REFERENCES

1. M. Gecevicius, R. Drevinskas, M. Beresna, and P. G. Kazansky, "Single beam optical vortex tweezers with tunable orbital angular momentum," Appl. Phys. Lett. **104**, 231110 (2014).
2. M. Ivanov and D. Hanstorp, "Controlled spin of a nonbirefringent droplet trapped in an optical vortex beam," Opt. Commun. **427**, 152 – 157 (2018).
3. D. N. Gupta, N. Kant, D. E. Kim, and H. Suk, "Electron acceleration to gev energy by a radially polarized laser," Phys. Lett. A **368**, 402 – 407 (2007).
4. V. Marceau, A. April, and M. Piché, "Electron acceleration driven by ultrashort and nonparaxial radially polarized laser pulses," Opt. Lett. **37**, 2442–2444 (2012).
5. S. Payeur, S. Fourmaux, B. E. Schmidt, J. P. MacLean, C. Tchervenkov, F. Légaré, M. Piché, and J. C. Kieffer, "Generation of a beam of fast electrons by tightly focusing a radially polarized ultrashort laser pulse," Appl. Phys. Lett. **101**, 041105 (2012).
6. E. A. Nanni, W. R. Huang, K.-H. Hong, K. Ravi, A. Fallahi, G. Moriena, R. J. D. Miller, and F. X. Kärtner, "Terahertz-driven linear electron acceleration," Nat. Commun. **6**, 8486 (2015).
7. V. G. Niziev and A. V. Nesterov, "Influence of beam polarization on laser cutting efficiency," J. Phys. D: Appl. Phys. **32**, 1455 (1999).
8. M. Kraus, M. A. Ahmed, A. Michalowski, A. Voss, R. Weber, and T. Graf, "Microdrilling in steel using ultrashort pulsed laser beams with radial and azimuthal polarization," Opt. Express **18**, 22305–22313 (2010).
9. R. Weber, A. Michalowski, M. Abdou-Ahmed, V. Onuseit, V. Rominger, M. Kraus, and T. Graf, "Effects of radial and tangential polarization in laser material processing," Phys. Procedia **12**, 21 – 30 (2011).
10. O. J. Allegre, W. Perrie, S. P. Edwardson, G. Dearden, and K. G. Watkins, "Laser microprocessing of steel with radially and azimuthally polarized femtosecond vortex pulses," J. Opt. **14**, 085601 (2012).
11. S. Quabis, R. Dorn, and G. Leuchs, "Generation of a radially polarized doughnut mode of high quality," Appl. Phys. B **81**, 597–600 (2005).
12. T. Wakayama, K. Komaki, Y. Otani, and T. Yoshizawa, "Achromatic axially symmetric wave plate," Opt. Express **20**, 29260–29265 (2012).
13. L. Marrucci, C. Manzo, and D. Paparo, "Optical spin-to-orbital angular momentum conversion in inhomogeneous anisotropic media," Phys. Rev. Lett. **96**, 163905 (2006).
14. S. Slussarenko, A. Murauski, T. Du, V. Chigrinov, L. Marrucci, and E. Santamato, "Tunable liquid crystal q-plates with arbitrary topological charge," Opt. Express **19**, 4085–4090 (2011).
15. M. Beresna, M. Gecevičius, and P. G. Kazansky, "Polarization sensitive elements fabricated by femtosecond laser nanostructuring of glass [invited]," Opt. Mater. Express **1**, 783–795 (2011).
16. M. Gecevicius, M. Ivanov, M. Beresna, A. Matijosius, V. Tamuliene, T. Gertus, A. Cerkauskaite, K. Redeckas, M. Vengris, V. Smilgevicius, and P. G. Kazansky, "Toward the generation of broadband optical vortices: extending the spectral range of a q-plate by polarization-selective filtering," J. Opt. Soc. Am. B **35**, 190–196 (2018).
17. E. J. Galvez, S. Khadka, W. H. Schubert, and S. Nomoto, "Poincaré-beam patterns produced by nonseparable superpositions of laguerre–gauss and polarization modes of light," Appl. Opt. **51**, 2925–2934 (2012).
18. C.-H. Yang, Y.-D. Chen, S.-T. Wu, and A. Y.-G. Fuh, "Independent manipulation of topological charges and polarization patterns of optical vortices," Sci. Rep. **6**, 31546 (2016).
19. P. Stanislovaitis, M. Ivanov, A. Matijosius, V. Smilgevicius, and T. Gertus, "Generation of radially polarized beams and higher order polarization singularities by optical parametric amplification of optical vortices," Opt. Eng. **56**, 095101 (2017).
20. X. Yi, X. Ling, Z. Zhang, Y. Li, X. Zhou, Y. Liu, S. Chen, H. Luo, and S. Wen, "Generation of cylindrical vector vortex beams by two cascaded metasurfaces," Opt. Express **22**, 17207–17215 (2014).
21. Z. Liu, Y. Liu, Y. Ke, Y. Liu, W. Shu, H. Luo, and S. Wen, "Generation of arbitrary vector vortex beams on hybrid-order poincare sphere," Photon. Res. **5**, 15–21 (2017).
22. A. D'Errico, M. Maffei, B. Piccirillo, C. de Lisio, F. Cardano, and L. Marrucci, "Topological features of vector vortex beams perturbed with uniformly polarized light," Sci. Reports **7**, 40195 (2017).
23. P. Stanislovaitis and V. Smilgevicius, "Control of optical vortex dislocations using optical methods," Lith. J. Phys. **52**, 295–300 (2012).
24. A. V. Volyar and T. A. Fadeeva, "Generation of singular beams in uniaxial crystals," Opt. Spectrosc. **94**, 235–244 (2003).
25. A. V. Volyar and T. A. Fadeeva, "Decay and fusion of polarization umbilics in a singular beam passed through a crystal," Opt. Spectrosc. **95**, 792–799 (2003).
26. E. Collett, *Field Guide to Polarization* (SPIE, P.O. Box 10, Bellingham, Washington 98227-0010 USA, 2005).